Factors contributing to the change in permeate quality upon temperature variation in nanofiltration

Citation: Roy, Yagnaseni, and John H. Lienhard. "Factors Contributing to the Change in Permeate Quality Upon Temperature Variation in Nanofiltration." Desalination 455 (April 2019): 58–70.

As Published: https://doi.org/10.1016/j.desal.2018.12.017

Publisher: Elsevier

Persistent URL: http://hdl.handle.net/1721.1/120312

Version: Author's final manuscript: final author's manuscript post peer review, without publisher's formatting or copy editing

Citation details: Y. Roy and J.H. Lienhard V, *Desalination*, vol. 455, pp. 58-79, 2019

(doi link: https://doi.org/10.1016/j.desal.2018.12.017)

Factors contributing to the change in permeate quality upon temperature variation in nanofiltration

Yagnaseni Roy[a], John H. Lienhard V[a,†]

Department of Mechanical Engineering, Massachusetts Institute of Technology, Cambridge, MA 02139-4307 USA

Abstract:

The selectivity of nanofiltration (NF) membranes is determined by membrane parameters as well as species mobilities (solute diffusivity and solvent viscosity). Changes in temperature affect each of these quantities, thereby altering membrane selectivity. To determine whether membrane parameters or mobilities primarily account for observed changes in permeate quality upon temperature increase, values of each property are either fitted from experimental data or calculated. Model validation with data from three feed compositions and two membranes reveals clear trends in temperature-dependent property-variation: pore size, net path length through membrane selective layer and negative membrane charge increase at higher temperature. An analytical approach is taken to explain the increase or decrease in permeate concentration due to each contributive factor, revealing the opposing effects of the two mobility factors. Modeling results further show that neither membrane parameter changes nor mobilities can alone explain selectivity changes with temperature. With increasing pressure, however, the net effect of membrane parameters increasingly overshadows that of the mobilities.

Key words: nanofiltration, temperature, membrane parameters, charge, diffusivity, viscosity

[†]**Corresponding author.** Email address: lienhard@mit.edu (J.H. Lienhard V)

Nomenclature

C	Concentration	$\mathrm{mol\ m^{-3}}$
C_X	Membrane charge	$\mathrm{mol\ m^{-3}}$
D_∞	Bulk diffusivity	$\mathrm{m^2 s^{-1}}$
F	Faraday constant	$\mathrm{C\ eq^{-1}}$
J_i	Ion flux	$\mathrm{mol\ m^{-2} s^{-1}}$
J_w	Water flux	$\mathrm{L m^{-2} h^{-1}}$
K_c	Hindrance factor for convective ion transport	
K_d	Hindrance factor for diffusive ion transport	
$\Delta P_{applied}$	Applied pressure	Pa
r_{pore}	Pore radius	m
R	Universal gas constant	$\mathrm{J mol^{-1} K^{-1}}$
T	Temperature	K
Δx_s	Effective path length through selective layer for the salt	m
z	Ion valence	

Greek symbols

γ	Activity coefficient	
δ_w	Effective path length through selective layer for water	m
ε_{pore}	Pore dielectric constant	
μ	Dynamic viscosity	$\mathrm{Pa-s}$
π	Osmotic pressure	Pa
σ	Reflection coefficient	
ϕ	Steric partitioning factor	
ϕ_B	Born solvation factor for partitioning	
ψ	Membrane potential	V
ω	Dummy variable	

Subscripts

f	Feed solution
D	Donnan potential
i	Ion
in	Pore entry
out	Pore exit
p	Permeate
$pore$	Inside the membrane pore
s	Salt
w	Water
∞	Bulk solution

1. Introduction

Nanofiltration (NF) is a pressure-driven membrane-based solution treatment method, similar to reverse osmosis (RO). Streams entering NF may occur over a wide range of temperatures, depending on the source. For example, effluents from textile, electroplating and pharmaceutical industries can range between 25-70^{o}C [1]–[4]. The introduction of specialty high temperature membranes by Dow in 2016 testifies to the practical significance of high temperature NF and RO [5]. Wilf et al. [6] report significant increase in water recovery ratio due to NF feed temperature increase (~3 fold from 25-55^{o}C for Dow's SR90 membrane). Consequently, heating the seawater is helpful both during winter, when the recovery ratio decreases, and in hybrid with thermal desalination systems such as multi-stage flash (MSF) and multi effect distillation (MED) [6], [7]. In the latter application, NF feed temperature of up to 55^{o}C for Arabian Gulf seawater is desirable to ensure a favorable trade-off between the increased water recovery ratio and diminished removal of scaling salts at higher feed temperature [6], [7]. Another application that NF has been proven useful for is zero liquid discharge (ZLD), especially for sulfate-rich industrial waste water. In most cases this waste water enters the NF system at 30-50^{o}C and sodium sulfate crystals are produced by NF or hybrid NF-evaporative crystallizer systems in a manner considered to be industrially attractive [8], [9].

While several examples in the literature discuss changes in salt rejection and water flux with change in temperature [10]–[12], relatively few explore why these changes occur. Because the temperature-dependence of solute diffusivity and solvent viscosity are well-studied, authors generally attribute reduced uncharged solute retention and increased solvent flux at higher temperature to the increased diffusivity and decreased solvent viscosity respectively [10], [11]. However, transport in NF is known to depend on various membrane properties, including pore size, membrane charge, and selective layer tortuosity [13], [14]. Therefore, accounting for temperature-induced changes of these membrane properties may be significant in explaining variations in NF selectivity due to temperature.

1.1. Previous studies on the effect of temperature on NF membranes

Previous work does discuss membrane properties in the context of temperature variation. Amar et al. [15] prove through their modeling work on uncharged solutes that only species mobilities (solute diffusivity and solvent viscosity) cannot account for the observed changes in rejection ratio with temperature change. References [2] and [16] qualitatively discuss pore radius change with temperature as a potentially significant contributor to selectivity changes. The study of charged species is more complicated than uncharged solutes: salt retention may stay unchanged, increase or decrease with temperature [10], [11], [17]. In reference [11], the negligible change in charged species removal percentage with temperature change is attributed to membrane charge, which was presumed to counteract the effect of increased ion diffusivity to reduce ion removal. Similar qualitative arguments were made in reference [16] to explain the near-constant potassium-chloride rejection ratio between 20-50^{o}C (transport of ionic species is affected by membrane charge) while the rejection ratio of glucose reduces significantly over the same range (affected primarily by diffusivity). However, the primary missing link in the literature is a quantitative analysis of the influence of each temperature-dependent parameter on permeate quality.

Our previous work, reference [18], explained the effect of temperature on individual ion transport modes in NF, i.e. diffusion, convection and electromigration, as well as the effect of temperature on partitioning mechanisms. That work discussed the relative contributions of membrane parameters vs. mobilities. The present paper elucidates the relative effect of individual parameters as well as sub-groups of parameters (mobilities vs. membrane parameters, structural parameters vs. charge-based membrane parameters) on transport through the membrane, as a result of temperature changes. More specifically, this paper investigates the change in permeate concentration (an increase of which indicates reduction in permeate quality and vice versa), since this quantity is the more practically relevant result (as opposed to solute transport values in reference [18]).

1.2. Current objectives: relative effect of temperature-dependent parameters on permeate quality

When temperature changes, various temperature-dependent factors cause both water flux and salt flux to change, thereby affecting permeate concentration (see Section 4.3). Consequently, the decrease in water viscosity at higher temperatures not only increases water flux, but also affects permeate quality. With respect to membrane properties, both structural aspects of the membrane and membrane charge may change with temperature. The current literature is unclear as to whether the change in species mobilities (water viscosity and ion diffusivity) or membrane properties with temperature change affect permeate quality more significantly. Furthermore, the change in membrane charge with temperature has been studied and modeled previously [19], [20], but there is lack of clarity on the magnitude of this effect relative to membrane structure changes or mobilities. The present work studies the effects of individual membrane properties and species mobilities, as well as various groups of parameters (membrane properties vs. mobilities and membrane structural properties vs. charge), on NF selectivity. Conclusions are drawn based on results from three feed compositions and two membranes, and the results are explained using an analytical framework. Changes in membrane selectivity will be characterized by changes in salt permeate concentration, since this quantity directly indicates permeate quality.

2. Governing Equations

The governing equations for species transport in nanofiltration (NF) are implemented numerically using MATLAB vR2016a for this work. These equations together constitute the Donnan Steric Pore Model (DSPM) and are summarized in Table 1 [21]. Successful use of this model for NF has been widely reported [19], [21]–[25]. A modification of the DSPM model that includes an additional exclusion mechanism, the dielectric exclusion mechanism, is considered in section 4.6; the governing equations, which include this effect, are given in Appendix A.

For all experimental data sets studied, concentration polarization is considered negligible, hence Eq. 2 in Table 1 uses the bulk feed concentration $C_{i,f}$ (this assumption is further discussed in section 3). The expression for the reflection coefficient σ (Eq. 5) applicable to charged species is derived by Bandini et al. [26]. Temperature dependence of solute diffusivity, $D_{i,\infty}$, is accounted for by the Stokes-Einstein equation [18], [27] and values of the dynamic viscosity of water, μ_w, are taken from reference [28].

Table 1: Governing equations for species transport in NF

Equation	Significance	
$J_i = -D_{i,\infty} K_{i,d} \frac{dC_{i,pore}}{dx} - \frac{z_i F}{RT} D_{i,\infty} K_{i,d} C_{pore} \frac{d\psi}{dx} + K_{i,c} C_{i,pore} J_w$	Ion flux	(1)
$\left. \frac{\gamma_{i,pore} C_{i,pore}}{\gamma_{i,f} C_{i,f}} \right\|_{in} = \phi_i \exp\left(-\frac{z_i F}{RT} \Delta\psi_{D,f} \right) \Big\|_{in}$	Extent of ion partitioning by membrane between feed solution and pore-entry	(2)
$\left. \frac{\gamma_{i,pore} C_{i,pore}}{\gamma_{i,p} C_{i,p}} \right\|_{out} = \phi_i \exp\left(-\frac{z_i F}{RT} \Delta\psi_{D,p} \right) \Big\|_{out}$	Extent of ion partitioning by membrane between pore-exit and permeate solution	(3)
$\left(\sum_{all\ ions} z_i C_{i,pore} \right) + C_X = 0$	Electroneutrality inside membrane pores	(4)
$J_w = \frac{r_{pore}^2}{8\mu_w \delta_w} (\Delta P_{applied} - \sigma \Delta\pi)$	Water flux	(5)
$J_s = J_w C_{s,p}$	Salt flux in pressure-driven membrane processes, in terms of J_w and $C_{s,p}$	(6)
$\Rightarrow \frac{dC_{s,p}}{C_{s,p}} = \frac{dJ_s}{J_s} - \frac{dJ_w}{J_w}$	Change in $C_{s,p}$ in terms of changes in J_s and J_w, following differentiation of Eq. 6	(7)

3. Validation with experimental data and temperature-dependent parameter change

As shown in Fig. 1, the model was validated for the lowest and highest temperatures for 4 data sets: 0.001 M NaCl (with the TFCS membrane by Koch Fluid Systems [19]); and 0.1 M NaCl, 0.1 M Na_2SO_4, and 0.001 M NaCl (the last three data sets used the Desal5DK membrane by GE Osmonics [20]). These four data sets are named A, B, C and D respectively. Validation and temperature-dependent parameter values for data set D are shown in this section and section 4.1 respectively, to support the trends of variation reported, but section 4.2 onwards discusses only data sets A to C, since numerical instabilities occurred for data set D while varying sub-sets of parameters as required in those sections.

Table 2 provides a summary of the reference data sets. Pore radii at each temperature were taken from the associated references, and values for δ_w were obtained from rearranging Eq. 5. The two fitting parameters were Δx_s and C_X and unique pairs of optimal values for each data set were obtained after minimizing the least square error on salt flux. This fitting procedure is similar to that of Sharma et al. [19] and hence comparable values of these parameters are obtained (Fig. 2).

As mentioned in section 2, concentration polarization (CP) is considered negligible for all data sets. The applicability of this assumption is inferred from the source literature themselves [19], [20]. Reference [19], from which data set A was taken, explicitly mentions that their experiments were designed to minimize concentration polarization such that the concentration near the membrane on the feed side can be closely approximated at a value equal to that of the bulk feed solution. The authors cite their previous works [29], [30] in which the same experimental setup was used and concentration polarization was considered negligible. Reference [20], from which data sets B, C and D were taken, uses the bulk feed concentration, $C_{i,f}$, in their equation for partitioning (as in Eq. 2 of section 2 of the present work), thereby inferring no CP in their work. Moreover, reference [27] by the same authors using the same crossflow cell explicitly mentions that due to the large crossflow velocity (1.23 ms^{-1}) CP was negligible. A similar crossflow velocity (1.27 ms^{-1}) was used in the same cell for the modeled data sets (from reference [20]). All references by the authors of reference [20] using their crossflow cell also neglect CP [31], [32]. Although the effect of temperature on CP is expected to be significant, and is relevant for most industrial applications, CP will be dependent on specific flow conditions and module geometry. Accounting for those effects is beyond the scope of the present work. The present work elucidates the relative contributions of membrane parameters and mobilities on permeate quality with temperature variation.

Table 2: Summary of experimental data sources:

Data set	Reference	Feed composition	Membrane	Temperatures	Highest applied pressure
A	[19]	0.001M NaCl	TFCS	5°C and 35°C	7.5 bar
B	[20]	0.1M NaCl	Desal5DK	22°C and 50°C	15 bar
C	[20]	0.1M Na_2SO_4	Desal5DK	22°C and 50°C	15 bar
D	[20]	0.001M NaCl	Desal5DK	22°C and 50°C	15 bar

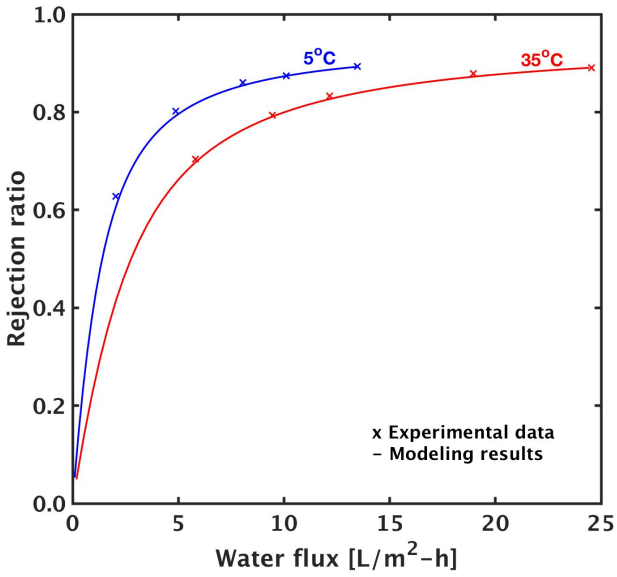

Fig. 1a

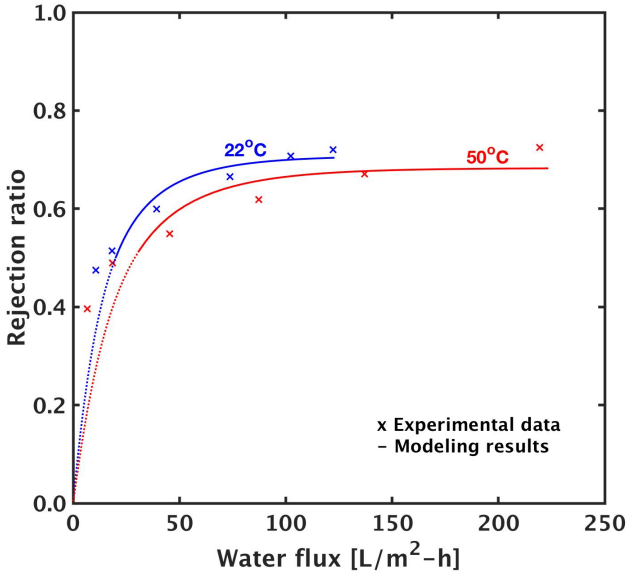

Fig. 1b

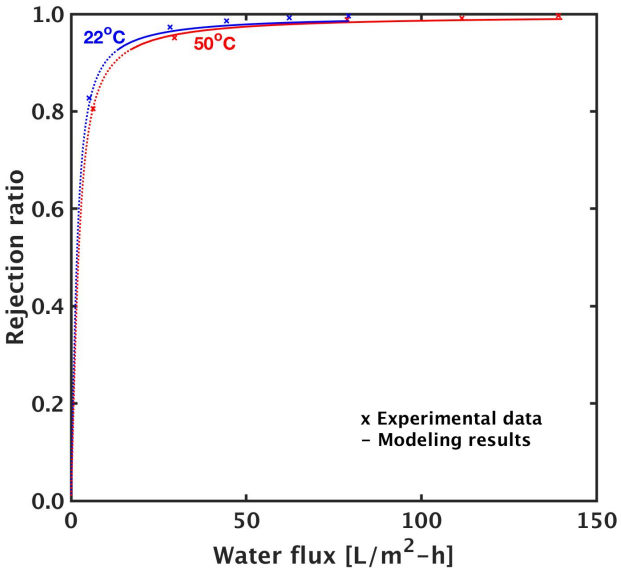

Fig. 1c

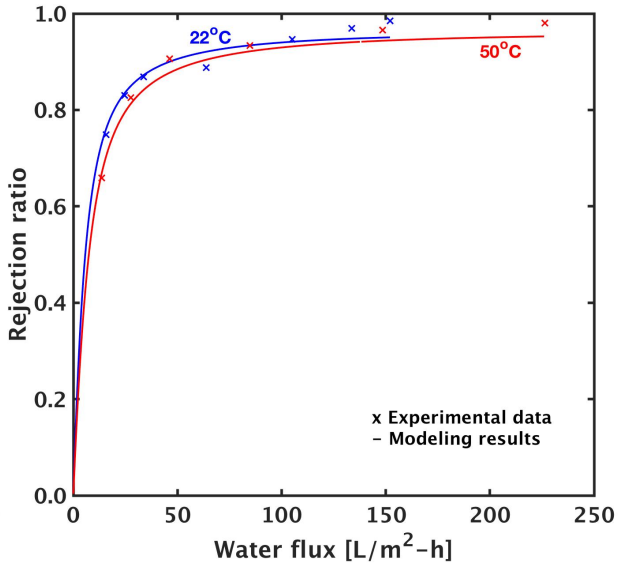

Fig. 1d

Figure 1. Model validation for data sets A, B, C and D (Figs. 1a-d respectively)

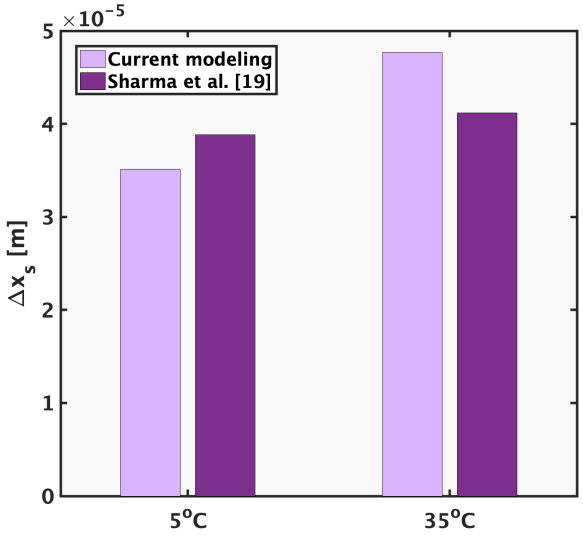

Fig. 2a

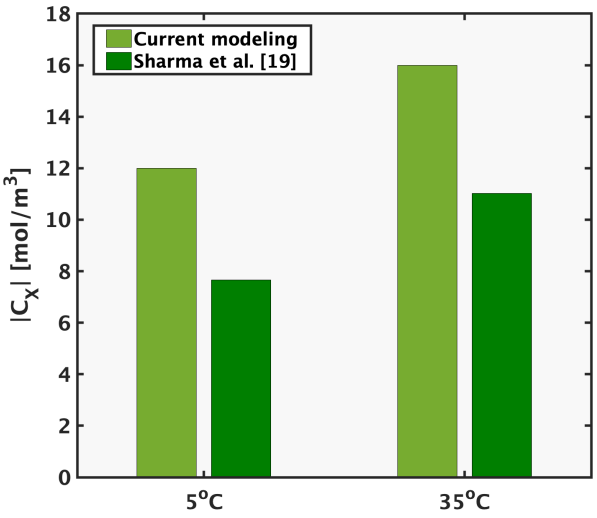

Fig. 2b

Fig 2. The two independent fitting parameters obtained in the current work are comparable to those in reference [19] by Sharma et al. for the same experimental data set (data set A).

4. Results and discussion

In this section, trends in membrane property variation due to temperature increase common to data sets A-D will first be shown (section 4.1). Subsequently, in sections 4.2-4.6, changes in salt permeate concentration, $C_{s,p}$, due to changes in temperature-dependent parameters will be discussed and explained. For instance, the contribution of membrane parameters to changes in $C_{s,p}$ will be shown in certain sections. In those sections, only changes in membrane parameters at the higher temperature (illustrated in section 3) will be implemented in the model, and the corresponding permeate concentration plotted. Similarly, the contribution of mobilities to permeate concentration refers to $C_{s,p}$ values when only mobilities $\left(\mu_w \text{ and } D_{i,\infty}\right)$ are changed to higher temperature values. This work focuses on permeate concentration because permeate quality (measured by concentration of solute species) is the focus of treatment methods like NF. As mentioned earlier, results for data set D are not shown in section 4.2 onwards due to numerical instability while varying sub-sets of parameters.

4.1. Change in membrane properties due to temperature increase

Upon fitting with all considered data sets, temperature-dependent trends are obtained. As shown in Fig. 3, net path length through the selective layer of both water and salt $(\delta_w \text{ and } \Delta x_s)$, and the magnitude of negative membrane charge, increased due to temperature increase. The increase in path length for all species is explained by the increase in selective layer tortuosity [33], and the larger membrane charge is due to the combined effect of enhanced anion-adsorption and membrane functional-group dissociation at higher temperatures. These mechanisms are discussed in further detail in section 4.5.

An increase in pore radius with temperature rise is commonly reported [15], [19], [27], [34] and is also observed for the current data sets. Values for pore size were taken from the reference literature containing the experimental data (reproduced in Appendix B) and were obtained by fitting with uncharged solute data by those authors.

The morphological changes as well as the increase in membrane charge, due to a combination of co-ion adsorption and functional group dissociation, together manifest as an endothermic character of the membrane's response to an increase in temperature [19]. As shown in Fig. 3c, the membrane charge predicted for data set C is significantly higher than the other data sets. Although such high charges predicted by the DSPM have been reported for NF membranes [35], the use of the DSPM-DE model (section 4.6) reduces the apparent magnitude of charge to a range more commonly reported for NF [14], [36].

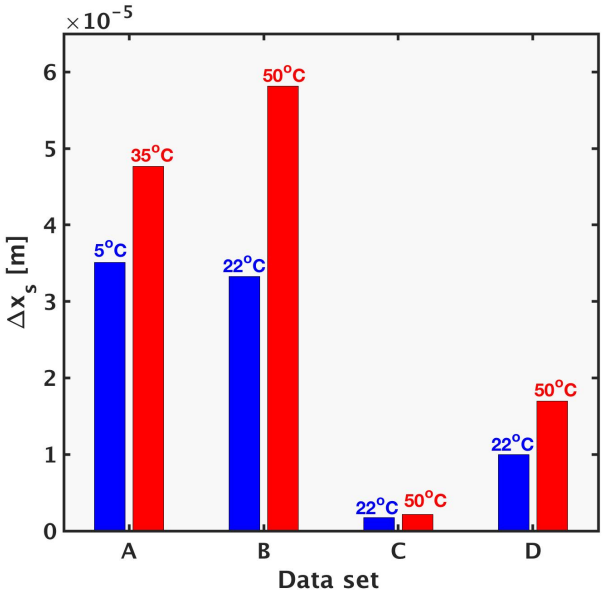

Fig. 3a

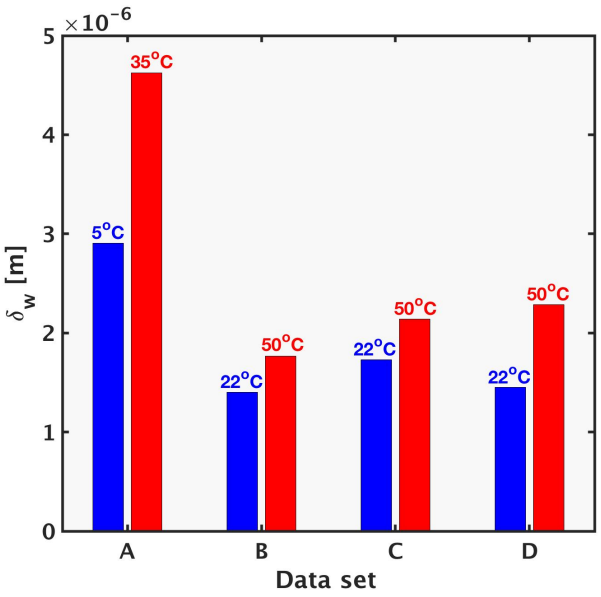

Fig. 3b

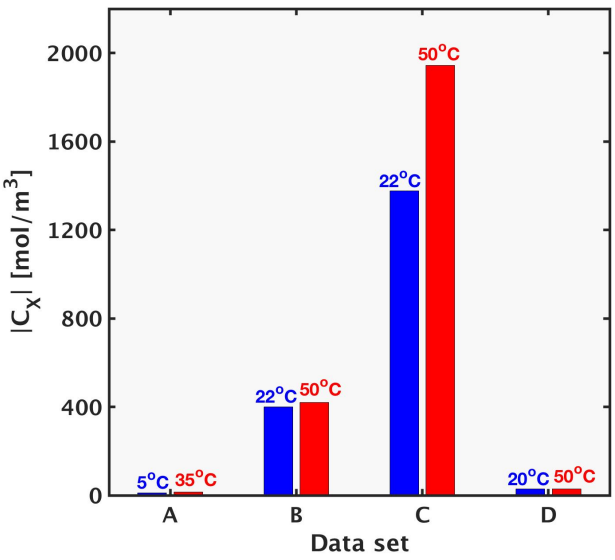

Fig. 3c

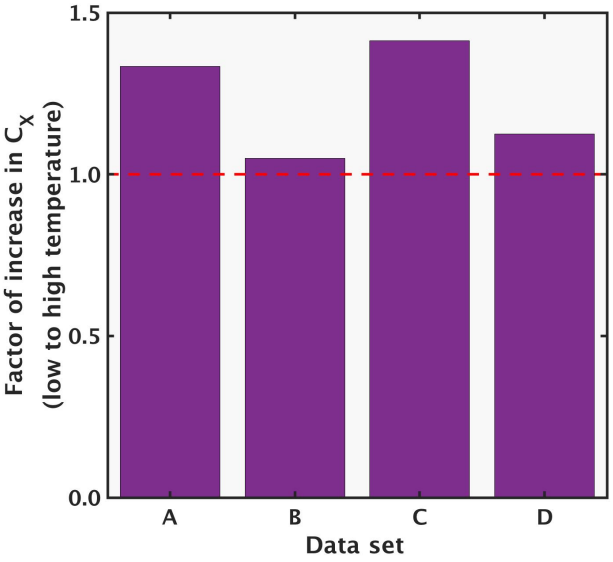

Fig. 3d

Fig 3. For all data sets (A-D), the same trends due to temperature variation were obtained: increase in pore size, δ_w, Δx_s and magnitude of negative membrane charge, $|C_X|$.

4.2. Temperature-based changes in membrane properties and mobilities each alter $C_{s,p}$ noticeably

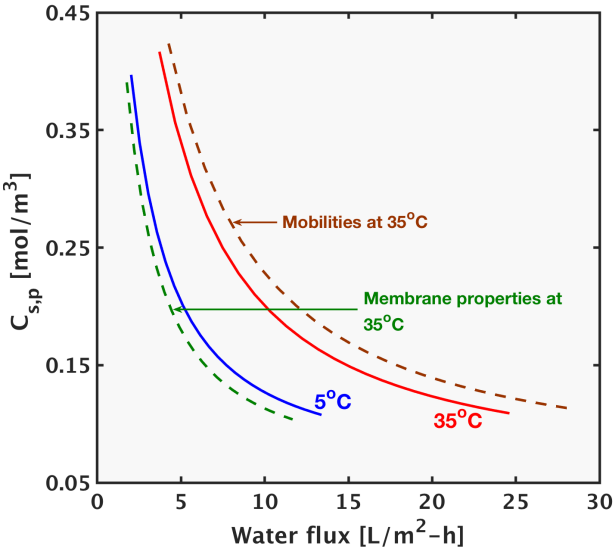

Fig. 4a

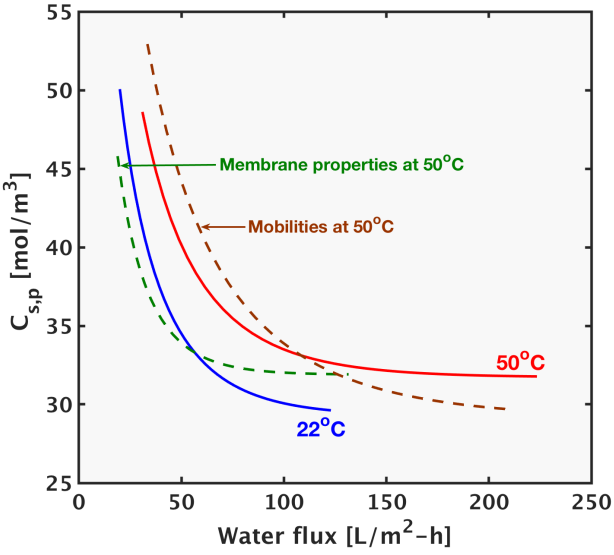

Fig. 4b

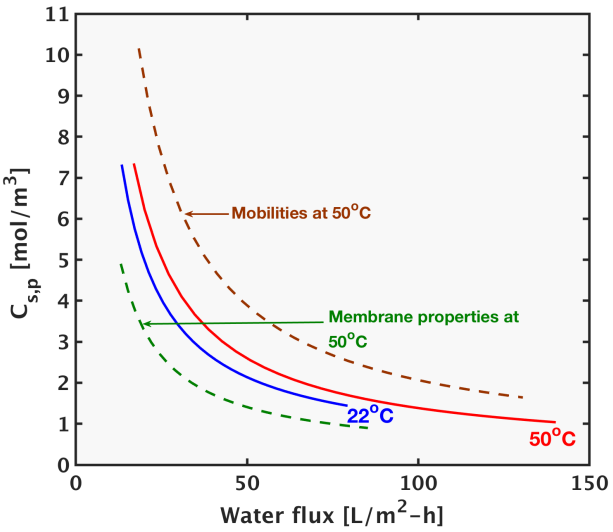

Fig. 4c

Fig 4. For all data sets (A-C), neither the membrane parameters nor mobilities could by themselves account for the net change in permeate quality from low to higher temperature. Along with the $C_{s,p}$ curves for the low and high temperature for each data set, two other lines are shown: 1. the curve obtained from changing mobilities to values at the higher temperature (holding membrane properties at lower temperature values); and 2. The curve obtained by changing membrane parameters at higher temperature values (holding mobilities constant). Since neither one of these lines are coincident with the higher temperature line, both sets of parameters need to be accounted for during temperature variant studies.

The results shown in this section (Fig. 4) were produced in two steps. First, permeate concentration, i.e. $C_{s,p}$, values were obtained for each data set by changing the mobilities ($D_{i,\infty}$ and μ_w) to their corresponding values at the higher temperature (Table 2) while the membrane parameters were kept at values corresponding to the lower temperature. The dashed maroon line in Fig. 4 shows the modeling results for the permeate concentration $C_{s,p}$ over a range of pressure, up to the highest value used in the source of experimental data (references [19], [20]). Subsequently, the dark green dashed line was produced by changing all membrane parameters ($r_{pore}, \delta_w, \Delta x_s$ and C_X) to their higher temperature values, while the mobilities were returned to their lower temperature values. Values of $C_{s,p}$ at the low and high temperature obtained after validation (section 3) are shown by the blue and red lines respectively.

For all data sets, the change in $C_{s,p}$ from low to high temperature could not be explained by either the membrane parameters or the mobilities by themselves. The increase in $D_{i,\infty}$ at the higher temperature increases the permeate concentration and is the dominant contribution, between the two mobility factors (explained further in the next section). Consequently, for data set A and C, and a large range of B, the mobilities line not only lies above the lower temperature line, but also exceeds the higher temperature values. The cumulative contribution of the membrane parameters in almost all cases reduces $C_{s,p}$ below the lower temperature line.

4.3. Analytical framework to explain the influence of temperature-dependent parameters on $C_{s,p}$

This section develops a simple analytical approach to predict the increase or decrease of permeate concentration due to any of the mobilities ($\mu_w, D_{i,\infty}$) or membrane properties ($r_{pore}, \delta_w, \Delta x_s, C_X$). Results from data set A will be used to illustrate the framework, and the same explanations hold for other data sets. Equation 6 (Table 1) shows the expression for salt flux in terms of water flux and permeate concentration applicable to pressure-driven membrane processes, such as NF and RO. Equation 7 (Table 1) gives the differential form of Eq. 6.

The differential form states that the relative change in permeate concentration $\left({dC_{s,p}}/{C_{s,p}}\right)$ is determined by a competition between the relative changes in salt flux $\left({dJ_s}/{J_s}\right)$ and water flux $\left({dJ_w}/{J_w}\right)$ (the relative change ratios can also be interpreted as percentage changes in each quantity due to change in an operating condition, such as temperature). For example, due to a given change in operating condition, if the salt flux increases to a greater extent (percentage) than the water flux, the permeate concentration of the salt will increase. This framework can be used to analyze the influence of each temperature-dependent parameter on $C_{s,p}$. The relative changes $\left({dC_{s,p}}/{C_{s,p}}\right)$ and $\left({dJ_s}/{J_s}\right)$ can be interpreted as percentage changes in the respective quantities: $\left({\Delta C_{s,p}}/{C_{s,p}}\right)$ and $\left({\Delta J_s}/{J_s}\right)$ (as discussed in Eqs. 8, 9 and Fig. 5). Figure 5 shows each term in Eqs. 8 and 9, which are equations derived by implementing Eq. 7 for the salt diffusivity and water viscosity, respectively (the bar plot for the percentage change in J_w due to $D_{i,\infty}$ is too small to be visible).

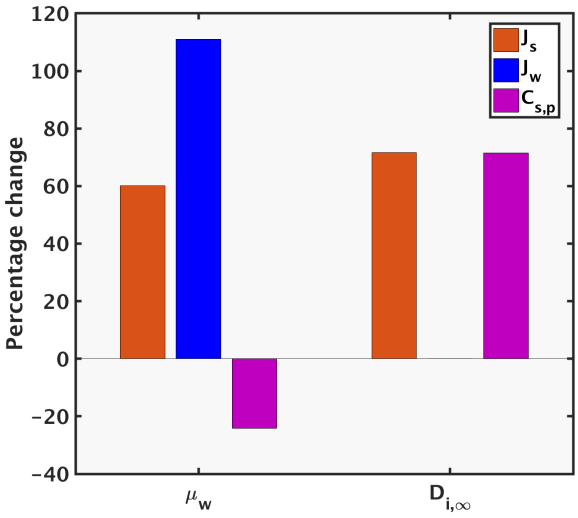

Fig. 5

Fig 5. Each term in Eqs. 8 and 9 is represented, as derived by implementing Eq. 7 for ion diffusivity, $D_{i,\infty}$, and water viscosity, μ_w, respectively. The terms in Eqs. 8 and 9 each show percentage change in salt flux, J_s, and water flux, J_w, when the respective mobility parameter values are changed from values at

the low temperature to the higher temperature (results in this figure are for data set A, in which those temperatures are 5°C and 35°C respectively).

Figure 6 shows the permeate concentration when each parameter is varied individually (to their high temperature values). At a fixed water flux value, the change in $C_{s,p}$ is solely due to change in salt flux (referring to Eq. 7, if $dJ_w = 0, \frac{dC_{s,p}}{C_{s,p}} = \frac{dJ_s}{J_s}$). Consequently, at any water flux value along the x-axis, Fig. 6a is best interpreted as the change in salt permeation with temperature. While Fig. 6a shows results over the range of operating pressure values, Figs. 6b and c provide a breakdown of Fig. 6a. Figures 6b and c show the changes in $C_{s,p}$ and J_w respectively at the highest operating pressure (referring to section 3, the highest pressure for data set A is 7.5 bar). Of particular interest in Figs. 6b and c is the increase or decrease (positive or negative value on bar plot respectively) of the permeate concentration $C_{s,p}$ and the water flux J_w due to each modeling parameter. While the magnitudes of change in $C_{s,p}$ and J_w due to each parameter (represented by the bars) are expected to be different for different data sets, the direction (positive or negative) for each parameter is the same for all data sets. These trends are explained in this section.

The diffusion coefficient, $D_{i,\infty}$, primarily increases the ion fluxes (and hence salt flux). Its influence on the water flux is negligible in comparison, occurring through a change in permeate osmotic pressure (Eq. 5). Consequently, Eq. 7 can be re-written as Eq. 8 to explain the influence of $D_{i,\infty}$ on salt permeate concentration. The notation $D_{s,\infty|5^oC} \rightarrow D_{s,\infty|35^oC}$[1] indicates that only effects due to the change in salt diffusivity from the initial temperature to a higher temperature (5 to 35°C) is accounted for.

$$\underbrace{\left.\frac{\Delta C_{s,p}}{C_{s,p}}\right|_{D_{s,\infty|5^oC}\rightarrow D_{s.\infty|35^oC}}}_{\%\ change\ in\ C_{s,p}\ due\ to\ D_{s,\infty}} \approx \underbrace{\left.\frac{\Delta J_s}{J_s}\right|_{D_{s,\infty|5^oC}\rightarrow D_{s,\infty|35^oC}}}_{\%\ change\ in\ J_s\ due\ to\ D_{s,\infty}} > 0 \tag{8}$$

As shown by Eq. 8, the resulting effect of $D_{s,\infty}$ with an increase in temperature is to increase permeate concentration (Fig. 5 shows each term in Eq. 8). The increase in $C_{s,p}$ due to the effect of $D_{s,\infty}$ by itself is shown in Fig. 6a, since the line for '$D_{i,\infty}$ at 35°C' lies above the 5°C line. The same trend is seen in Fig. 6b, where the bar plot for ion diffusivity shows a positive value. On the other hand, the almost negligible effect of $D_{i,\infty}$ on water flux, J_w, is clear from Fig. 6c, since the water flux barely changed when only the ion diffusivity was changed to its value at 35°C (while all other modeling parameters were kept at values corresponding to 5°C).

$$\left.\frac{\Delta C_{s,p}}{C_{s,p}}\right|_{\mu_{w|5^oC}\rightarrow\mu_{w|35^oC}} = \left.\left(\frac{\Delta J_s}{J_s} - \underbrace{\frac{\Delta J_w}{J_w}}_{dominant}\right)\right|_{\mu_{w|5^oC}\rightarrow\mu_{w|35^oC}} < 0 \tag{9}$$

[1] In this discussion, the net salt diffusivity, $D_{s,\infty}$, is used synonymously with ion diffusivity $D_{i,\infty}$, since the model takes individual ion diffusivities, but the increase in each ion's diffusivity results in an increase in the salt's diffusivity.

The solvent viscosity appears in Eq. 5. Accordingly, a decrease in μ_w with an increase in temperature has the effect of increasing solvent flux. The dominant term in Eq. 9 is the relative change in J_w, even though $\left({}^{dJ_s}/_{J_s}\right)$ is also affected by the change in water flux. The result is a decrease in $C_{s,p}$ due to the temperature-induced decrease in solvent viscosity. The decrease in $C_{s,p}$ due to the viscosity of water is clear in Figs. 6b, where the bar plot for this parameter has a negative value, in contrast to that of the ion diffusivity. The significant effect of μ_w on increasing water flux, J_w, is shown in Figs. 5 and 6c. (As mentioned earlier, Fig. 5 represents the percentage change terms used in Eqs. 8 and 9, while Fig. 6c shows the change in water flux due to each parameter).

Like $D_{i,\infty}$, the membrane parameters Δx_s and C_X primarily affect $\left({}^{dJ_s}/_{J_s}\right)$. However, the temperature-induced changes in both of these parameters result in decreased J_s, and hence decreased $C_{s,p}$. The influence of δ_w is explained similarly to that of μ_w, although the increase in its magnitude with temperature by itself reduces J_w $\left({}^{\Delta J_w}/_{J_w} < 0 \Rightarrow {}^{\Delta C_{s,p}}\Big/_{C_{s,p}} > 0\right)$. The increase in r_{pore} with temperature increases both $C_{s,p}$ (due to lowered steric hindrance) and J_w (Eq. 5), hence increasing J_s (Eq. 6). Consequently, the increase in r_{pore} with temperature increase results in $C_{s,p}$ increase, as shown in Eq. 10. For all data sets studied, Eq. 10 holds, and hence the pore radius increase due to temperature increase causes a decrease in permeate quality, as shown in Fig. 6a and b. Figures 5 and 6 explain the changes in J_s, J_w and $C_{s,p}$ due to each of the membrane parameters, and the reasoning is similar to that of the mobilities, as discussed above.

$$\left({}^{\Delta J_s}/_{J_s} > {}^{\Delta J_w}/_{J_w}\right)\Big|_{r_{pore|5^oC} \to r_{pore|35^oC}} \Rightarrow \Delta C_{s,p}\big|_{r_{pore|5^oC} \to r_{pore|35^oC}} > 0 \qquad (10)$$

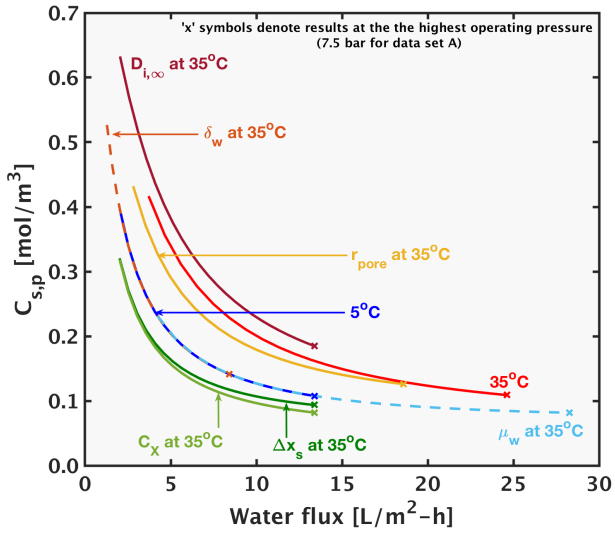

Fig. 6a

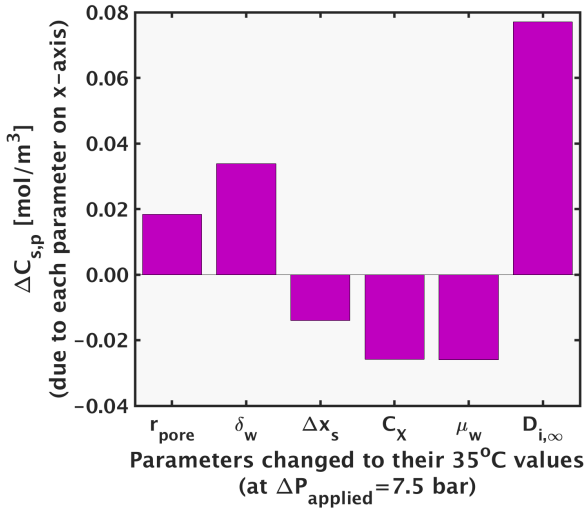

Fig. 6b

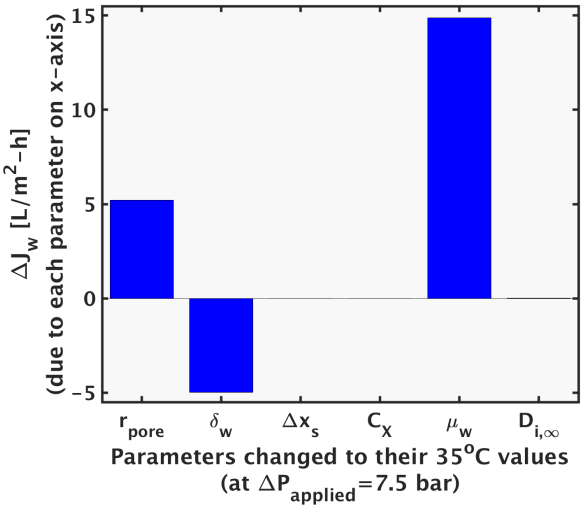

Fig. 6c

Fig 6. Fig. 6a: Effect of individual parameters on permeate concentration (data set A). Each line is obtained by fixing the labelled parameter to its value at 35°C, while all other model inputs are at the lower temperature (5°C) values. The × symbols in 6a indicate results at the highest operating pressure, 7.5 bar. The change in $C_{s,p}$ at a fixed J_w is an indication of the change in salt permeability with temperature (referring to Eq. 7, if $dJ_w = 0, \frac{dC_{s,p}}{C_{s,p}} = \frac{dJ_s}{J_s}$). Figures 6b and c: These figures show a breakdown of Fig. 6a at the highest operating pressure. Figures 6b and 6c respectively show the $C_{s,p}$ and J_w changes due to each parameter separately. Of particular interest is the increase or decrease (positive or negative sign on bar) of $C_{s,p}$ and J_w due to each parameter. These trends of increase or decrease of $C_{s,p}$ due to each parameter are similar for all other data sets.

4.4. Dominance of membrane parameters over mobilities with increasing pressure

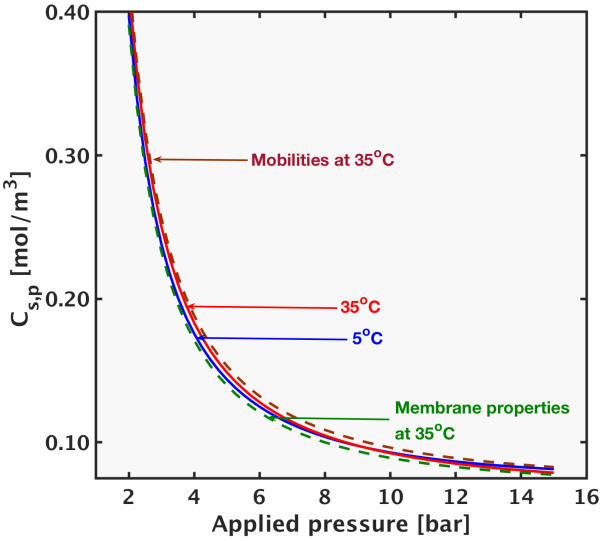

Fig. 7a

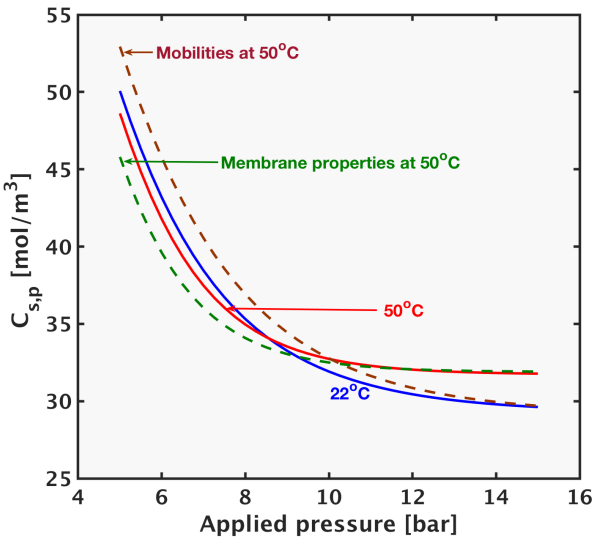

Fig. 7b

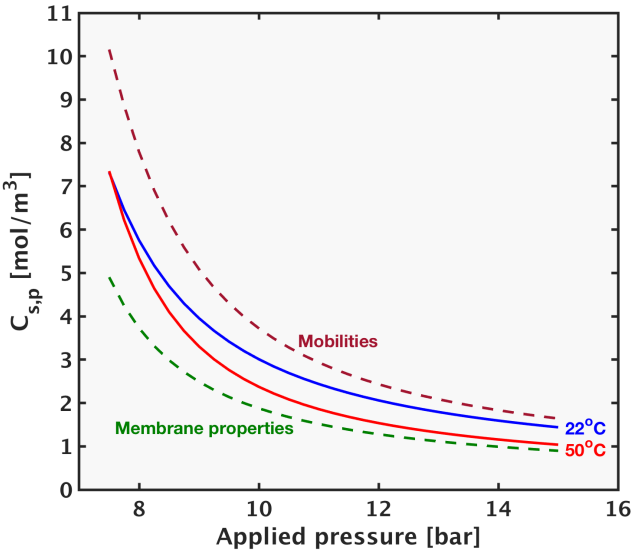

Fig. 7c

Fig 7. For all data sets (A-C), the net effect (magnitude of change in $C_{s,p}$) due to membrane parameters supersedes that due to mobilities at increasing applied pressure values.

Figure 7 shows the variation of $C_{s,p}$ against applied gauge pressure up to 15 bar. Results by Sharma et al. [19] have been extended to 15 bar using the fitting parameters obtained during validation. As commonly shown in the NF literature, rejection ratio increases with water flux (and therefore applied pressure) and reaches a plateau at a certain maximum value [14], [15]. Accordingly, the permeate concentration, $C_{s,p}$, decreases with water flux (and applied pressure), subsequently reaching a minimum plateau value. Due

to the decrease in value of $C_{s,p}$, the corresponding value of $\Delta C_{s,p|\omega_{|22^oC}\rightarrow\omega_{|50^oC}}$(where ω is a dummy variable and can be any one of the mobilities or membrane parameters) reduces. An analogous situation is that the difference between 20 and 10 is 10, but the difference between 2 and 1 is 1. i.e. the difference between two smaller numbers results in a smaller number.

As shown in Fig. 6b, between the two mobility factors, μ_w and $D_{i,\infty}$, the magnitude of deviation in permeate concentration from values at lower temperature are more significant due to $D_{i,\infty}$. Accordingly, $\left|\Delta C_{s,p}\right|\!|_{D_{i,\infty|22^oC}\rightarrow D_{i,\infty|50^oC}} \gg \left|\Delta C_{s,p}\right|\!|_{\mu_{w|22^oC}\rightarrow\mu_{w|50^oC}}$. As the pressure increases and $\Delta C_{s,p|\omega_{|22^oC}\rightarrow\omega_{|50^oC}}$ reduces in magnitude, the total contribution of the mobility factors reduces. Consequently, the line contributed by the mobilities lies above the lower temperature line in all cases, but almost merges with the lower temperature line as the applied pressure increases.

4.5. Improved selectivity at higher temperature - overcoming unfavorable membrane property changes

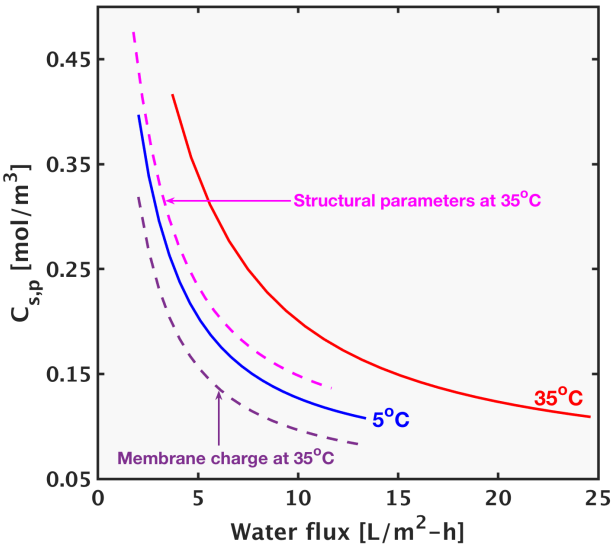

Fig. 8a

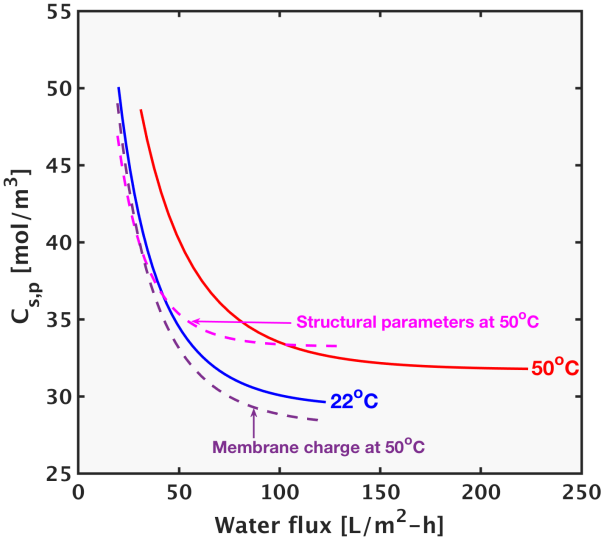

Fig. 8b

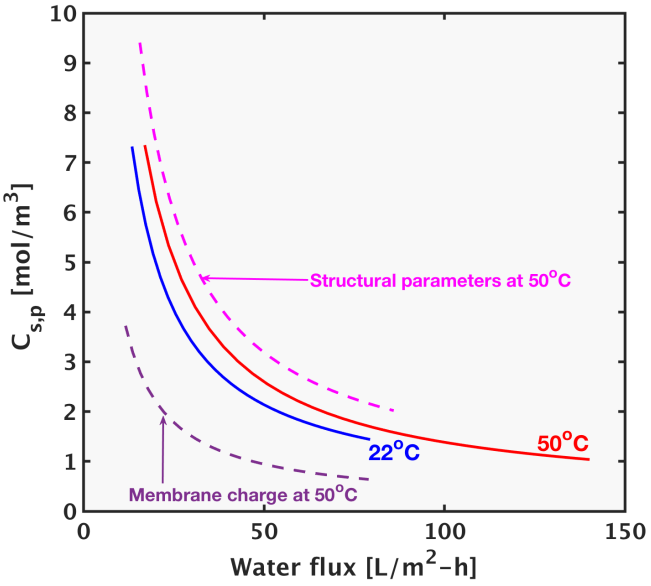

Fig. 8c

Fig 8. In general, changes in structural properties ($r_{pore}, \delta_w, \Delta x_s$) at higher temperature result in increased in permeate concentration (reduced permeate quality), while the increased magnitude of membrane charge lowers permeate concentration. Consequently, membrane material and structure that reduces propensity to re-structure at higher temperature, as well as membrane material with higher anion-adsorption tendency with increasing temperature would maintain high permeate quality at elevated temperatures.

Results shown in this section were obtained from the model by first keeping mobilities and membrane charge at values corresponding to the lower temperature for each data set (Table 2), while structural parameters (r_{pore}, δ_w and Δx_s) were changed to the higher temperature values. The resulting modeling values are shown by the dashed magenta line in Fig. 8. Subsequently, the dashed purple line in Fig. 8 was obtained by fixing the mobilities and structural parameters at the lower temperature values and changing the membrane charge to its value at the higher temperature.

As shown in Fig. 8, for all data sets, the temperature-based changes in structural parameters cumulatively result in increased $C_{s,p}$ (worsened permeate quality). As may be inferred from Fig. 6, this increase in $C_{s,p}$ was due to the effect of increased pore radius and the effective travel length for water with temperature increase (the increased travel length for the salt has the effect of reducing $C_{s,p}$). On the other hand, the increase in negative membrane charge at higher temperature lowers the permeate concentration (improved permeate quality).

These conclusions suggest that membrane-design for higher temperature applications requires a focus on minimizing the structural changes in the membrane, i.e. to reduce structural reorientation of the membrane polymer. On the other hand, the increase in membrane charge at the higher temperature (section 3) proved advantageous for permeate quality. Hence, improved anion-adsorption propensity at higher temperature, resulting in higher membrane charge is a desirable quality.

One method to reduce material restructuring upon temperature increase is the introduction of crystalline domains that act as 'physical cross-linkers' (i.e., effectively acting as clamps) to minimize polymer-reorientation with temperature change. Such crystalline domains were identified in the Desal5DK membrane by Amar et al. [27]. Previous literature has reported difference in charge acquiring propensity in solution for different membranes [37]. A possible explanation for enhanced ion-adsorption in some membranes is larger hydrophilicity; however, better understanding of the involved mechanism is hindered by the often-proprietary nature of membrane chemistries.

4.6. Similar predictions using DSPM and DSPM-DE models on the contributive factors to $C_{s,p}$ change with temperature

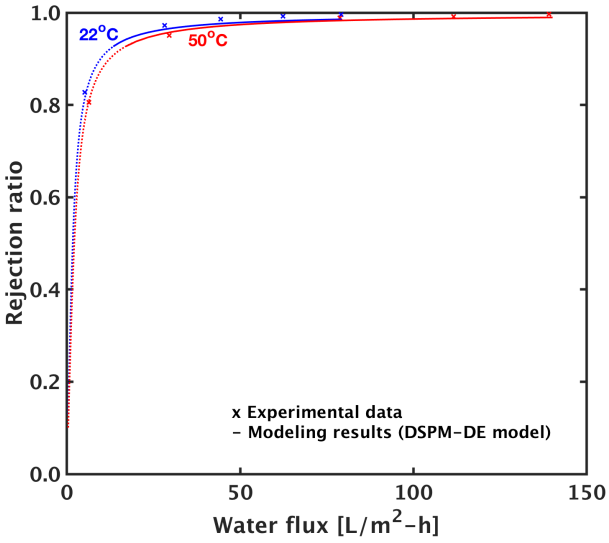

Fig. 9a

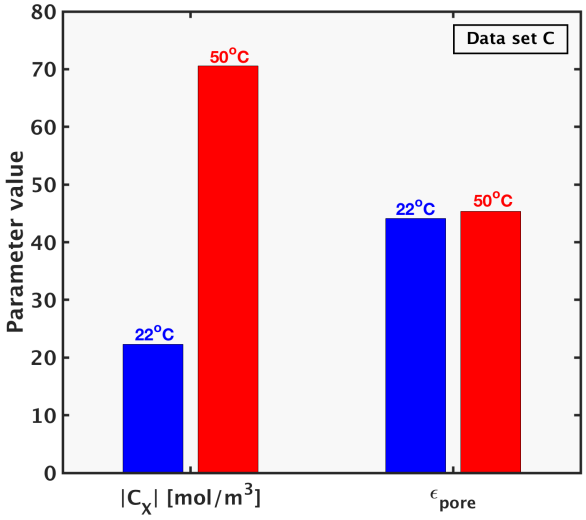

Fig. 9b

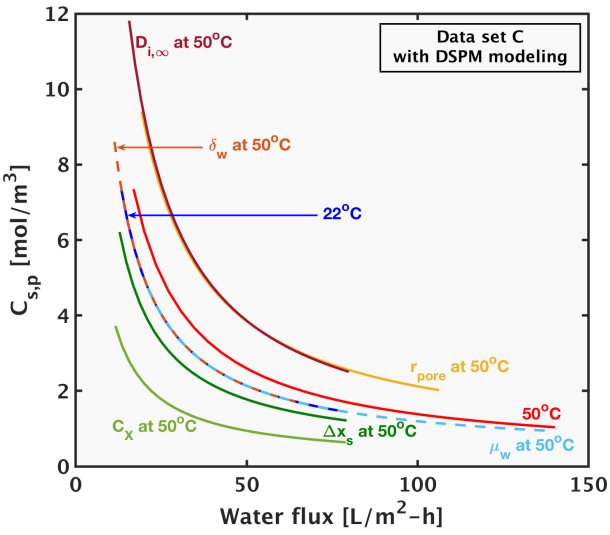

Fig. 9c

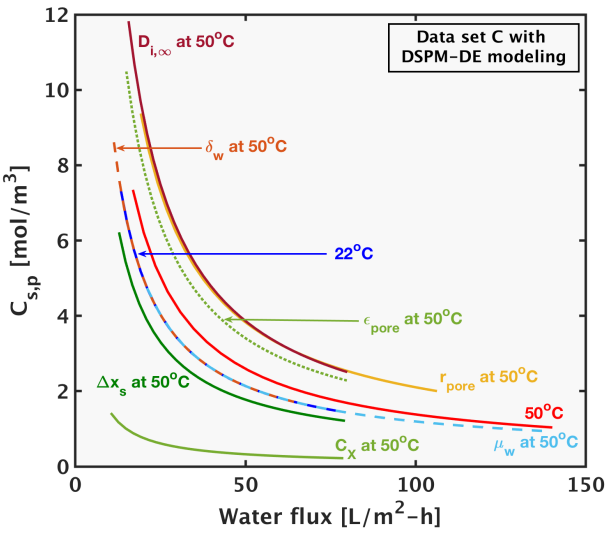

Fig. 9d

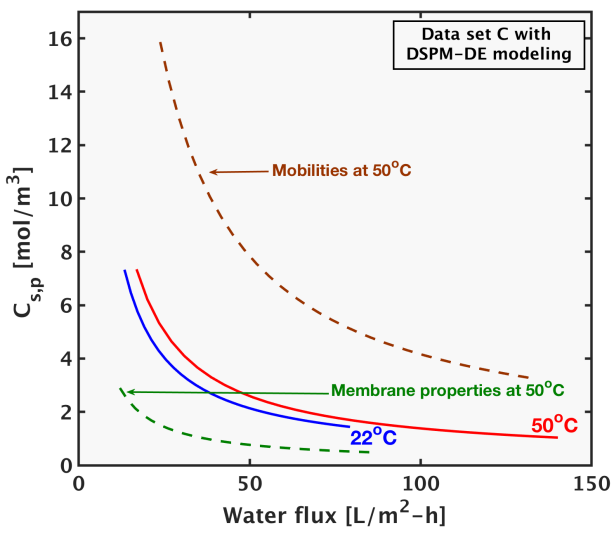

Fig. 9e

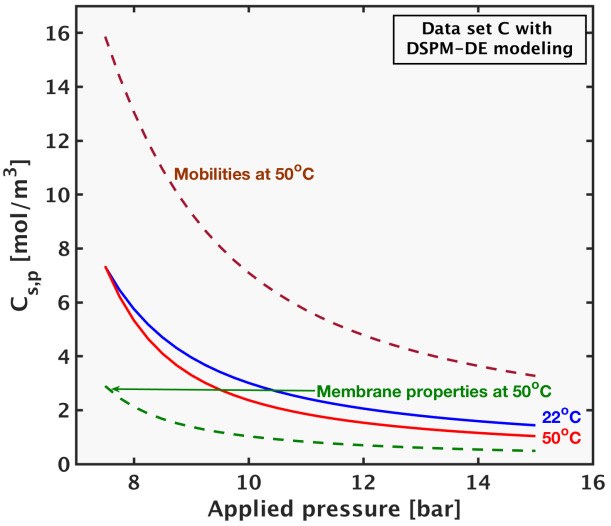

Fig. 9f

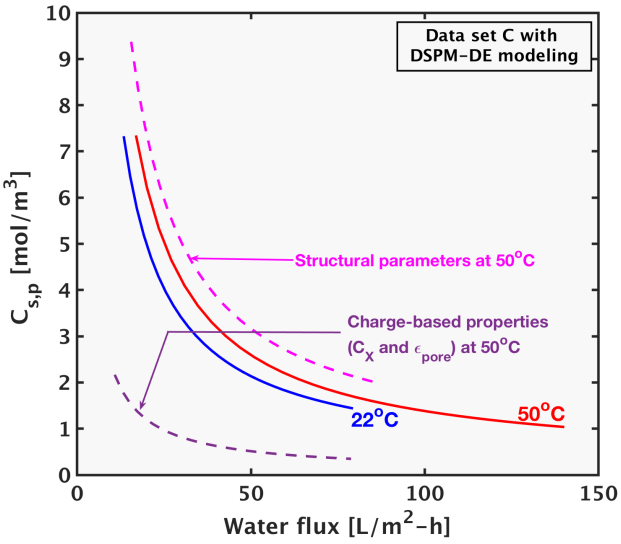

Fig. 9g

Fig 9. Results for data set C using the DSPM-DE model, an updated version of the DSPM, are shown. The conclusions from sections 4.2 to 4.5 hold: i) neither membrane parameters nor mobilities can fully account for change in NF performance with temperature; ii) membrane parameters are increasingly dominant over the mobilities with increasing pressure; and iii) the membrane structural parameters and charge-based properties decrease and increase permeate quality respectively.

The DSPM-DE model is an updated version of the DSPM and includes the dielectric exclusion mode of ion exclusion along with the Donnan and size-based effects [14], [23]. The partitioning equations (Eqs. 2 and 3) with this mechanism included are in accordance with references [13], [14], [18], [23] and are

reproduced in Appendix A. Due to the incorporation of the dielectric exclusion mechanism, the membrane charge predicted by the DSPM-DE model to achieve validation with experimental results is lower than those predicted by the DSPM (represented in Fig. 3c) [14], [35].

In this section, results on data set C using the DSPM-DE model will be shown, since this model reduced the predicted value of membrane charge to a range more common for NF [14], [36]. Similar to reference [18], the values of the pore dielectric constant are estimated from the expression introduced by Bowen and Welfoot [14], so that this parameter is not treated as an additional independent fitting parameter (Fig. 9b). The values obtained for the Desal5DK membrane using this approach at 22 and 50°C respectively in reference [18] are 44.11 and 45.37.

The conclusions from sections 4.2 to 4.5 remain valid when the DSPM-DE is used: as shown in Fig. 9, the membrane parameters are increasingly dominant over the mobilities with increasing pressure and the structural properties cumulatively worsen permeate quality while the charge-based properties cumulatively improve permeate quality. However, as shown in Fig. 9c, the increase in magnitude of the pore dielectric constant with temperature causes an increase in $C_{s,p}$ due to ε_{pore} by itself. Upon comparison of Figs. 9e and 9f with 4c and 7c respectively, the line for $C_{s,p}$ due to only the change in mobility values to values at 50°C is slightly shifted. Although the model agreement with experiments using the DSPM-DE model (Fig. 9a) is similar to that using the DSPM (Fig. 1c), the non-linearity of the governing equations modeling causes the results using dielectric exclusion to be marginally different from those using DSPM. The difference is barely visible under most circumstances (compare Fig. 9c with 9d and 8c and 9g), but is noticeable for Figs 9e and f (compare with Figs 4c and 7c respectively).

5. Conclusions

Conclusions from this study are as follows:

1. Membrane parameters each change with temperature increase: pore size, net species path length, and membrane charge increase in magnitude.
2. Neither the set of membrane parameters nor mobilities by themselves can account for change in membrane selectivity with temperature variation.
3. The changes in solvent viscosity and ion diffusivity (the mobilities) decrease and increase permeate concentration with increasing temperature respectively, thereby partially cancelling each other's effects. The influence of ion diffusivity is dominant and hence the net effect of the mobilities is to increase permeate concentration at higher temperature.
4. At larger pressures, the change in permeate concentration due to each membrane parameter and mobility factor is diminished. Consequently, the net contribution of the two mobilities is superseded by the membrane parameters, which account for almost the total change in permeate concentration due to temperature change.
5. Generally, the membrane structural changes and changes in membrane charge with increase in temperature cause increase and decrease of the permeate concentration, respectively. Improved salt retention at higher temperatures can be attained by reducing the membrane material's

tendency to restructure, as well as using material with higher anion-adsorption or functional group dissociation propensity at elevated temperatures.

6. References

[1] X. Chai, G. Chen, P.-L. Yue, and Y. Mi, "Pilot scale membrane separation of electroplating waste water by reverse osmosis," *J. Memb. Sci.*, vol. 123, pp. 235–242, 1997.

[2] Y. K. Ong, F. Y. Li, S. P. Sun, B. W. Zhao, C. Z. Liang, and T. S. Chung, "Nanofiltration hollow fiber membranes for textile wastewater treatment : Lab-scale and pilot-scale studies," *Chem. Eng. Sci.*, vol. 114, pp. 51–57, 2014.

[3] L. Yao, L. Zhang, R. Wang, S. Chou, and Z. L. Dong, "A new integrated approach for dye removal from wastewater by polyoxometalates functionalized membranes," *J. Hazard. Mater.*, vol. 301, pp. 462–470, 2016.

[4] "WATER TECHNOLOGY FUTURES : A global blueprint for innovation," in *Singapore International Water Week*, 2016.

[5] "Product Data Sheet DOW ™ Specialty Membrane XUS290508 and XUS290504 Nanofiltration Elements," 2016.

[6] M. Wilf, L. Awerbuch, C. Bartels, M. Mickley, G. Pearce, and N. Voutchkov, "Nanofiltration technology and applications," in *The guidebook to membrane desalination technology*, no. 66, L'Aquila: Desalination publications, 2007, pp. 243–454.

[7] L. Awerbuch, M. Parker, and I. Agha-Mourad, "Integrated Upgrading of Thermal Processes and Nanofiltration Experience of SEWA Project," *IDA World Congr. Gran Canar. Spain*, 2007.

[8] G. Bargeman, M. Steensma, A. ten Kate, J.B. Westerink, R.L.M. Demmer, H. Bakkenes, C.F.H. Manuhutu, "Nanofiltration as energy-efficient solution for sulfate waste in vacuum salt production," *Desalination*, vol. 245, no. 1–3, pp. 460–468, 2009.

[9] E. Curcio, X. Ji, A.M. Quazi, S. Barghi, G.D. Profio, E. Fontananova, T. Macleod, E. Drioli, "Hybrid nanofiltration – membrane crystallization system for the treatment of sulfate wastes," *J. Memb. Sci.*, vol. 360, pp. 493–498, 2010.

[10] J. Schaep, B. Van der Bruggen, S. Uytterhoeven, R. Croux, C. Vandecasteele, D. Wilms, E, Van Houtte, and F. Vanlerberghe, "Removal of hardness from groundwater by nanofiltration1," *Desalination*, vol. 119, no. 1–3, pp. 295–301, 1998.

[11] M. Mänttäri, A. Pihlajamäki, E. Kaipainen, and M. Nyström, "Effect of temperature and membrane pre-treatment by pressure on the filtration properties of nanofiltration membranes," *Desalination*, vol. 145, no. 1–3, pp. 81–86, 2002.

[12] M. J. H. Snow, D. de Winter, R. Buckingham, J. Campbell, and J. Wagner, "New techniques for extreme conditions: high temperature reverse osmosis and nanofiltration," *Desalination*, vol.

105, no. 1–2, pp. 57–61, 1996.

[13] Y. Roy, M. H. Sharqawy, and J. H. Lienhard, “Modeling of flat-sheet and spiral-wound nanofiltration configurations and its application in seawater nanofiltration,” *J. Memb. Sci.*, vol. 493, pp. 360–372, 2015.

[14] W. R. Bowen and J. S. Welfoot, “Modelling the performance of membrane nanofiltration — critical assessment and model development,” *Chem. Eng. Sci.*, vol. 57, no. 7, pp. 1121–1137, 2002.

[15] N. Ben Amar, H. Saidani, A. Deratani, and J. Palmeri, “Effect of temperature on the transport of water and neutral solutes across nanofiltration membranes,” *Langmuir*, vol. 23, no. 6, pp. 2937–2952, 2007.

[16] M. Nilsson, G. Tragardh, and K. Ostergren, “The influence of pH, salt and temperature on nanofiltration performance,” *J. Memb. Sci.*, vol. 312, no. 1–2, pp. 97–106, 2008.

[17] A. Hangi, A. Mohebbi, M. Mirzaei, and H. Kaydani, “Evaluation and Comparison of Sulfate Anions Removal from Artificial and Industrial Wastewaters by Nanofiltration Process in a Laboratory Scale,” *J. Membr. Sep. Technol.*, vol. 4, no. September, pp. 40–52, 2015.

[18] Y. Roy, D. M. Warsinger, and J. H. Lienhard, “Effect of temperature on the solute transport in nanofiltration : diffusion, convection and electromigration,” *Desalination*, vol. 420C, pp. 241–257, 2017.

[19] R. R. Sharma and S. Chellam, “Temperature and concentration effects on electrolyte transport across porous thin-film composite nanofiltration membranes: Pore transport mechanisms and energetics of permeation,” *J. Colloid Interface Sci.*, vol. 298, no. 1, pp. 327–340, 2006.

[20] N. Ben, H. Saidani, J. Palmeri, and A. Deratani, “Effect of temperature on the rejection of neutral and charged solutes by Desal 5 DK nanofiltration membrane,” *Desalination*, vol. 246, no. 1–3, pp. 294–303, 2009.

[21] K. P. Lee, G. Bargeman, R. De Rooij, A. J. B. Kemperman, and N. E. Benes, “Interfacial polymerization of cyanuric chloride and monomeric amines: pH resistant thin film composite polyamine nanofiltration membranes.,” *J. Memb. Sci.*, vol. 523, no. September 2016, pp. 487–496, 2017.

[22] A. Kowalik-Klimczak, M. Zalewski, and P. Gierycz, “Prediction of the chromium (III) separation from acidic salt solutions on nanofiltration membranes using donnan and steric partitioning pore (DSP) model.,” *Archit. Civ. Eng. Environ.*, vol. 9, no. 3, pp. 135–140, 2016.

[23] V. Geraldes and A. M. Brites Alves, “Computer program for simulation of mass transport in nanofiltration membranes,” *J. Memb. Sci.*, vol. 321, no. 2, pp. 172–182, 2008.

[24] W. R. Bowen, J. S. Welfoot, and P. M. Williams, “A linearised transport model for nanofiltration: development and assessment,” *AIChE J*, vol. 48, no. 4, p. 760, 2002.

[25] W. R. Bowen and A. W. Mohammad, “Diafiltration by nanofiltration: Prediction and optimization,” *AIChE J.*, vol. 44, no. 8, pp. 1799–1812, 1998.

[26] S. Bandini and V. Morelli, “Effect of temperature, pH and composition on nanofiltration of mono/disaccharides: Experiments and modeling assessment,” *J. Memb. Sci.*, vol. 533, no. December 2016, pp. 57–74, 2017.

[27] H. Saidani, N. Ben Amar, and J. Palmeri, “Interplay between the Transport of Solutes Across Nanofiltration Membranes and the Thermal Properties of the Thin Active Layer,” *Langmuir*, vol. 26, no. 4, pp. 2574–2583, 2010.

[28] M.L. Huber, R.A. Perkins, A. Laesecke, D.G. Friend, J.V. Sengers, M.J. Assael, I.N. Metaxa, E. Vogel, R. Mareš, K. Miyagawa, “New international formulation for the viscosity of H2O,” *J. Phys. Chem. Ref. Data*, vol. 38, no. 2, pp. 101–125, 2009.

[29] R. R. Sharma, S. Chellam, “Temperature Effects on the Morphology of Porous Thin Film Composite Nanofiltration Membranes,” *Environ. Sci. Technol.*, vol. 39, no. 13, pp. 5022–5030, 2005.

[30] R. R. Sharma, R. Agrawal, and S. Chellam, “Temperature effects on sieving characteristics of thin-film composite nanofiltration membranes: Pore size distributions and transport parameters,” *J. Memb. Sci.*, vol. 223, no. 1–2, pp. 69–87, 2003.

[31] R. Moliner-Salvador, A. Deratani, J. Palmeri, and E. Sánchez, “Use of nanofiltration membrane technology for ceramic industry wastewater treatment,” *Bol. la Soc. Esp. Ceram. y Vidr.*, vol. 51, no. 2, pp. 103–110, 2012.

[32] N. Ben Amar, N. Kechaou, J. Palmeri, A. Deratani, and A. Sghaier, “Comparison of tertiary treatment by nanofiltration and reverse osmosis for water reuse in denim textile industry,” *J. Hazard. Mater.*, vol. 170, no. 1, pp. 111–117, 2009.

[33] R. Sharma and S. Chellam, “Temperature effects on the transport of water, uncharged and charged solutes across polymeric nanofiltration membranes,” in *American Water Works Association Membrane Technology Confernce*, 2007, pp. 17–20.

[34] H. Q. Dang and W. E. Price, “The effects of feed solution temperature on pore size and trace organic contaminant rejection by the nanofiltration membrane NF270,” vol. 125, pp. 43–51, 2014.

[35] N. S. Kotrappanavar, A. A. Hussain, M. E. E. Abashar, I. S. Al-Mutaz, T. M. Aminabhavi, and M. N. Nadagouda, “Prediction of physical properties of nanofiltration membranes for neutral and charged solutes,” *Desalination*, vol. 280, no. 1–3, pp. 174–182, 2011.

[36] C. Labbez, P. Fievet, A. Szymczyk, A. Vidonne, A. Foissy, and J. Pagetti, “Analysis of the salt retention of a titania membrane using the ‘DSPM’ model: Effect of pH, salt concentration and nature,” *J. Memb. Sci.*, vol. 208, no. 1–2, pp. 315–329, 2002.

[37] J. M. M. Peeters, M. H. V. Mulder, and H. Strathmann, “Streaming potential measurements as a characterization method for nanofiltration membranes,” *Colloids Surfaces A Physicochem. Eng. Asp.*, vol. 150, no. 1–3, pp. 247–259, 1999.

7. Appendix A

The governing equations for ion partitioning between the membrane and solution when dielectric exclusion is included in the modeling are given in Table A.1. Dielectric exclusion due to the Born effect is considered in this work; this approach has been used successfully in several other works [13], [14], [23], [35]. In Eqs. A.3 and A.4, the terms $\Delta G_i, k_B, r_{i,Stokes}, e_0, \varepsilon_0$ represent the Gibbs free energy of solvation, the Boltzmann's constant, Stokes radius of the ion, the electronic charge and the vacuum permittivity respectively. The term $\varepsilon_{solution}$ in Eq. A.4 represents the dielectric constant of the solution in contact with the membrane, and depending on its use in either Eq. A.1 or A.2, it represents the feed or permeate dielectric constants respectively.

$\left.\frac{\gamma_{i,pore} C_{i,pore}}{\gamma_{i,f} C_{i,f}}\right\|_{in} = \phi_i \phi_B \exp\left(-\frac{z_i F}{RT}\Delta\psi_{D,f}\right)\Big\|_{in}$	Extent of ion partitioning by membrane between feed solution and pore-entry	(A.1)
$\left.\frac{\gamma_{i,pore} C_{i,pore}}{\gamma_{i,p} C_{i,p}}\right\|_{out} = \phi_i \, \phi_B \exp\left(-\frac{z_i F}{RT}\Delta\psi_{D,p}\right)\Big\|_{out}$	Extent of ion partitioning by membrane between pore-exit and permeate solution	(A.2)
$\phi_B = exp\left(\frac{-\Delta G_i}{k_B T}\right)$	Born solvation contribution for partitioning	(A.3)
$\Delta G_i = \frac{z_i^2 e_0^2}{8\pi\varepsilon_0 r_{Stokes}}\left(\frac{1}{\varepsilon_{pore}} - \frac{1}{\varepsilon_{solution}}\right)$	Born solvation energy barrier	(A.4)

8. Appendix B

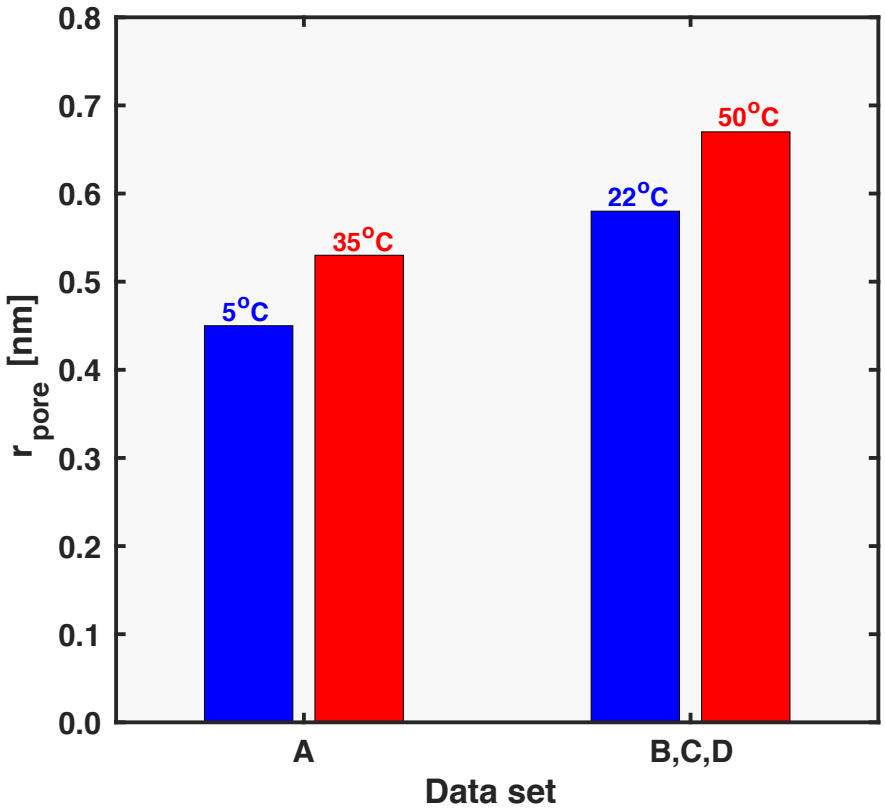

Fig. B.1: Pore sizes at the low and high temperature for the TFCS membrane used for data set A (obtained from reference [19]) and those for the Desal5DK membrane used for data sets B,C and D (obtained from reference [15]).